frontiers | Frontiers in Astronomy and Space Sciences

TYPE Brief Research Report
PUBLISHED 13 May 2025
DOI 10.3389/fspas.2025.1540522

Check for updates

OPEN ACCESS

EDITED BY
Fabio La Franca,
Roma Tre University, Italy

REVIEWED BY
Daniela Bettoni,
Osservatorio Astronomico di Padova (INAF), Italy
Alberto Nigoche-Netro,
University of Guadalajara, Mexico
Marina Trevisan,
Federal University of Rio Grande do Sul, Brazil

*CORRESPONDENCE
Nataša Bon,
nbon@aob.rs

RECEIVED 05 December 2024
ACCEPTED 23 April 2025
PUBLISHED 13 May 2025

CITATION
Bon N, Bon E, Marziani P and Popović LC (2025) Ratios of forbidden [OIII] λλ4959,5007 and [NII] λλ6548,6583 lines in nearby narrow emission line galaxies.
Front. Astron. Space Sci. 12:1540522.
doi: 10.3389/fspas.2025.1540522

Ratios of forbidden [OIII] λλ4959,5007 and [NII] λλ6548,6583 lines in nearby narrow emission line galaxies

Nataša Bon[1]*, Edi Bon[1], Paola Marziani[2] and Luka Č. Popović[1]

[1]Astronomical Observatory, Belgrade, Serbia, [2]Osservatorio Astronomico di Padova (INAF), Padua, Veneto, Italy

Galaxies with narrow emission lines play a crucial role in testing the theoretical values of transition probabilities, especially for lines that need conditions that are hard to produce in laboratory plasma, and hence the theoretical values could not be checked in experimental measurements. In this paper, we explore the [O III]$\lambda\lambda$4959,5007 and the [N II]$\lambda\lambda$6,548, 6,583 doublets and their line ratios in a volume limited samples ($0.01 \leqslant z \leqslant 0.05$) of Sy2, LINERs, composite objects and star-forming galaxies, that zooms in the central region of these objects. Our results confirm that the theoretical line ratios $R([OIII]) = 2.98$ and $R([NII]) = 3.05$ as predicted by Storey and Zeippen (2000) are consistent with observations of HII regions, for both line ratios. This agreement occurs under conditions minimally affected by reddening, corresponding to total-to-selective extinction ratios (R_V) between 3.1 and 4.1. In contrast, Seyfert 2, LINER, and composite galaxies confirm the same theoretical prediction of the [OIII] line ratios in the case of stronger reddening ($2.1 \leq R_V \leq 3.1$), while [NII] ratios stays slightly lower than predicted by Storey and Zeippen (2000), aligning more closer to the values reported by Galavis et al. (1997), or indicating a presence of environmental conditions that affects these line ratios. This discrepancy in [NII] ratios suggests that, beyond reddening effects, the physical conditions in the [NII]-emitting regions of active galaxies differ from those in HII regions. Shocks, variations in electron density, ionization mechanisms, and gas or dust composition may contribute to these differences.

KEYWORDS

galaxies, emission line galaxies, seyfert-galaxies, star forming galaxies, liners, active galaxies, emission lines ratio

1 Introduction

Emission lines from ionized gas regions in galaxies provide important diagnostic tools for understanding their physical properties. Two of the most widely studied sets of emission lines are the [O III]$\lambda\lambda$4959, 5007 Å and [N II]$\lambda\lambda$6548, 6583 Å lines.

The [OIII] λ4958.911 Å and λ5006.843 Å lines, originating from doubly ionized oxygen (O^{2+}), are traditionally associated with the narrow-line regions (NLRs) of AGNs, where they trace the ionized gas illuminated by the radiation from a central accreting supermassive black hole. However, these lines are also prevalent in star-forming regions and HII regions, where the gas is ionized by young, massive stars. Similarly, composite galaxies, which host both AGN activity and star formation, exhibit a mix of emission from these different ionization sources, making the interpretation of the [OIII] lines more complex. Theoretical calculations, such as those by GalavIs et al. (1997), predict a [OIII] λ5007/λ4959 flux ratio of 2.89, but observational studies often report slightly higher values, with measurements from Iye et al. (1987)]with a value of 3.17 for starburst, and Leisy and Dennefeld (1996) with a value of 3.00 for planetary nebulae. This discrepancy has been explored by Storey and Zeippen (2000), who introduced relativistic corrections to the magnetic dipole operator, bringing theoretical predictions closer to the observed values. Studying a sample of 62 AGN, (Dimitrijević et al., 2007), reported an [OIII] λ5007/λ4959 intensity ratio of 2.993 ± 0.014.

In addition to [OIII], the [NII]$\lambda\lambda$6548, 6583 lines play a similarly important role in tracing the ionization conditions in galaxies. The [NII] lines, produced by singly ionized nitrogen (N^+), are especially useful for distinguishing between different types of ionization sources, as their intensity relative to Hα is sensitive to both star formation and AGN activity. The theoretical expectations for [NII] line intensity ratio is about 3, and observational results are in agreement with that (see, for, e.g., Dojčinović et al., 2023, obtained 3.049 ± 0.021 for a sample of Seyfert 2 objectsDojcinovic.

To effectively classify galaxies based on their ionization sources, we rely on the Baldwin, Phillips, and Terlevich (BPT) diagram (Baldwin et al. (1981)), which uses line ratios such as [OIII]/Hβ, [NII]/Hα. The BPT diagram allows us to distinguish between star-forming galaxies, composite objects, LINER and Seyfert 2 (Sy2) galaxies. Each subgroup represents a different combination of ionization mechanisms: star-forming galaxies are dominated by photoionization from young stars, composite galaxies contain both star formation and AGN activity, and Sy2 galaxies are characterized by strong AGN-driven ionization.

Narrow emission lines observed in galaxy spectra are commonly attributed to photoionization of the interstellar medium (ISM) by energetic sources such as active galactic nuclei (AGNs) or young, massive stars within HII regions. In AGNs, narrow-line regions (NLRs) are photoionized by the hard radiation field of the accretion disk around the central supermassive black hole, producing prominent high-excitation lines. In contrast, in star-forming galaxies, narrow emission lines originate primarily from HII regions ionized by O- and B-type stars, typically associated with recent or ongoing star formation activity.

However, it is now recognized that other ionizing sources can also contribute significantly to the excitation of the gas. In addition to AGNs and young stellar populations, evolved low-mass stars - particularly hot post-asymptotic giant branch (post-AGB) stars and white dwarfs - can produce a hard ionizing continuum capable of generating LINER-like emission spectra. These stellar remnants, collectively known as HOLMES (hot low-mass evolved stars), may dominate the ionization budget in galaxies with little or no recent star formation (Binette et al., 1994; Stasińska et al., 2008; Byler et al., 2019). Their contribution is particularly relevant in early-type galaxies and systems with low specific star formation rates, where the emission-line excitation cannot be attributed to either AGN activity or massive stars alone.

In this study, we focus on analyzing the [OIII] λ5007/λ4959 and [NII] λ6583/λ6548 flux ratios across a large sample of nearby galaxies classified according to the BPT diagram.

2 Sample selection

The spectroscopic data used in this work were taken from the DR7 release of Sloan Digital Sky Survey (SDSS) (Abazajian et al., 2009). The SDSS survey provides spectra in the wavelength range 3,800–9,200 Å and with mean spectral resolution $\lambda/\Delta\lambda \sim$ 2,000, taken with 3 arcsec diameter fibers. We used upper limit of Petrosian r-band magnitude ($r^* < 17.77$) that corresponds to SDSS spectroscopic limit (Strauss et al., 2002). We restricted our sample to the objects for which the observed spectra show signal-to-noise (S/N) in SDSS g band higher than 30 [according to Bon et al. (2014)].

The aim was to investigate the gas component in the central region of the galaxy. Since galaxies were observed through a fixed angular fiber, we constrained the redshift range of the galaxies between 0.01 and 0.05, that corresponds to projected linear distances between 0.3 and 1.5 kpc from the galaxy center, or 0.6 and 3 kpc in diameter. We analyzed only those objects where redshift confidence, provided by SDSS DR7 database is higher than 0.95.

To firmly confine the FOV of the fiber only on the inner part of the galaxy, we constrained the size of the SDSS objects, using the SDSS isophotes in the r-band ("isoA_r"), which represents the size of the major axis of the galaxy. We bounded the major axis to be larger than 1 kpc, so the SDSS fiber covers the inner part of the galaxy.

In our study, we focused on the central region of galaxies to ensure that the observed emission lines predominantly originate from nuclear processes such as starburst activity or AGN ionization, rather than diffuse ionized gas from the outer regions. While it is well established that the central parts of galaxies often contain older stellar populations, we assumed that in the presence of an active nucleus or a nuclear starburst, strong emission lines from ionized gas would dominate the observed spectrum. This assumption is supported by previous studies showing that nuclear starbursts and AGN-related ionization effects are typically more intense in the central regions than in the outskirts (e.g., Kewley et al., 2006). By restricting our analysis to the central region, we aim to reduce the contribution of older stellar populations and extended diffuse emission, ensuring that our measurements primarily trace the physical conditions of the ionized gas in the nuclear region.

We constrained Hα and Hβ emission line characteristics in order to avoid high luminous galaxies and normal galaxies, and have only galaxies with nuclear activity in the sample. To do so, we selected from SDSS database objects where the equivalent width (EW) of the Hα and Hβ lines is higher than 2, since we noticed that emission lines whose EWs are between 0 and 2 are mainly in the noise level and are mainly classified as galaxies without emission lines. Since we were mostly interested in Narrow Emission Line Galaxies (hereafter, NELG), we constrained lower limits of line widths. Upper limits were chosen to avoid strong luminous galaxies. Therefore, we set the following constraints for the emission lines: 1.5 Å $<$ σ(Hα) $<$ 9 Å, 1 Å $<$ σ(Hβ) $<$ 7 Å and EW (Hα, $H\beta$) $>$ 2 Å.

The resulting sample contains 4510 NELG and does not include duplicates found in the original DR7 catalog. Also, there is no spurious detection (no object with Petrosian magnitude in z band higher than 22.83).

3 Methods

3.1 Analysis of a volume limited narrow emission line galaxy sample

In order to analyze simultaneously all components of the integrated light from selected objects, we used the ULySS[1] (Koleva et al., 2009) full spectrum fitting package, which fits spectroscopic observations against a bounded linear combination of nonlinear model components, convolved with a parametric line-of-sight velocity distribution.

The ULySS code was originally developed for studying the history of stellar populations and for analyzing stellar atmospheres. One of the main advantages of ULySS is its flexibility, allowing users to define arbitrary non-linear components, as explained in detail by Bon et al. (2014), Bon et al. (2016). In this study, we modified ULySS by introducing additional components designed to simultaneously fit the nebular continuum, stellar population templates, AGN continuum and a comprehensive set of emission lines. The parameters of the emission lines could be either tied or left free, depending on the specific fitting conditions.

For the purpose of studying spectra in NELG, the model of emission line galaxy used in the fit represents the linear combination of power law continuum, stellar population model convolved with a line-of-sight broadening function, and a sum of Gaussians, that represent emission lines, as described in Bon et al. (2014). The model is multiplied by a Legendre polynomial that supposes to absorb the errors in the flux calibration, Galactic extinction or any other cause that affects the shape of the continuum. The model is generated at the same resolution and with the same sampling as the observation. Spectra were fitted in the 3,700–6,800 Å wavelength range. The fit is performed in the pixel space.

We used Vazdekis stellar population models from the library of single stellar populations, computed with the MILES library and Salpeter IMF (Sánchez-Blázquez et al., 2006; Vazdekis et al., 2010).

By fitting a spectrum with the ULySS, we reconstruct the SSP-equivalent age and metallicity, mean stellar velocity and velocity dispersion, spectral index of the featureless continuum, shifts, widths and intensities of emission lines, as well as fractions of all model components.

For this study we fitted all Balmer lines and strong forbidden lines [O II]$\lambda\lambda$3727,3729, [O III]$\lambda\lambda$4959,5007, [N II]$\lambda\lambda$6548,6585, and [S II]$\lambda\lambda$6716,6732. We also included coronal lines like [Fe VII]λ6,087 and [Fe X]λ6,374, He IIλ4,686, and several other less prominent features when present.

In this work we analyzed only narrow emission lines, narrower than 600 km s^{-1}, so the profiles of emission lines were fitted with a single Gaussian function. Figure 1 represent examples of the fit in total fitted wavelength range, and zoomed Hβ and Hα domains in Sy2 galaxy. In the upper panels of the graphs, the black line represents the observed spectrum, the blue line represents the best fit model, and the red line the multiplicative polynomial, while the green, light red, and violet lines represent components of the best fit model: violet–stellar population, red–emission lines, and green–AGN continuum. The bottom panel represents residuals of the best fit (black line). The solid green lines mark the 1σ deviation, and the dashed line is the zero axis.

The common way of fitting [OIII]$\lambda\lambda$4959,5007 and [NII]$\lambda\lambda$6548,6583 lines is to tie their widths and to fix their intensities to ≈3. Here both width and intensity of Gaussians used to fit emission lines are free parameters in the fit, so we were able to analyze flux ratios of [OIII]$\lambda\lambda$4959,5007 and [NII]$\lambda\lambda$6548,6583 lines in four subclasses of NELG, and search for their differences.

Emission lines fluxes as well as their uncertainties were measured using IDL procedure INT_TABULATED from the best fit model of emission lines and residual of the fit, respectively.

Before measuring the flux ratios we removed from the set those spectra where: (a) relative error of line dispersion of any analyzed forbidden emission line is higher than 10%; (b) the difference between the width of two emission lines in the doublet [OIII]$\lambda\lambda$4959,5007 lines is higher than 20%; the same criteria is used for two [NII]$\lambda\lambda$6548,6583 lines; (c) relative error of the line flux is higher than 20%; and (d) overlap between [NII] 6,548 $\AA$ and Hα lines was higher than 1Å (to be as consistent as with the data set constrains of Dojčinović et al. (2023), where they selected spectra without overlapped emission lines).

In our analysis, each emission line was modeled using a single Gaussian profile. Even though the two lines of a forbidden doublet (e.g., [N II] $\lambda\lambda$6548, 6584 or [O III] $\lambda\lambda$4959, 5007) are physically expected to originate from the same ionized region and thus share similar kinematic properties, we chose not to tie their widths during the fitting process. Instead, we allowed the line widths to be fit independently and subsequently applied a post-fit consistency check: spectra in which the fitted widths of the two doublet components differed by more than 20% were excluded from the analysis. This approach was motivated by the relatively low spectral resolution of the SDSS data ($R \sim 1800$, corresponding to ~69–75 km s^{-1}), which can introduce fitting uncertainties, particularly when working with narrow and closely spaced lines. Enforcing tied widths under such conditions can sometimes lead to artificially poor fits or biased line fluxes due to local residuals or noise structures. Our adopted strategy allowed for greater fitting flexibility while ensuring that only physically plausible measurements-where the kinematics of the doublet components remain reasonably consistent-were retained for statistical analysis. We emphasize that the goal of this procedure was to retain empirical reliability without imposing potentially misleading constraints in low-resolution data.

We used this method for the statistical analysis of the spectra in the central kpc of the selected NELG. The narrow emission lines can be used to classify the dominant ionization energy source in emission line galaxies. Consequently we made the well known Hα/[NII]6548,6583$\AA$ vs. Hβ/[OIII]4959,5007$\AA$ BPT diagnostic diagram (Baldwin et al., 1981) to separate four classes of objects - Seyfert 2, LINERs, HII regions and so-called" composite objects "(Kewley et al., 2001; Kauffmann et al., 2003). By analyzing the BPT diagram, we distinguished 226 Sy2s, 89 LINERs, 3,117 starburst galaxies and 1,078 composite objects.

Therefore, from 229 Sy2s, 89 LINERs, 3,117 starburst galaxies and 1,078 composite objects, these additional constraints have limited our samples to 37 Sy2, 48 LINERs, 262 composite spectra and 1,227 starbursts for [OIII] ratio analysis, while for the case of [NII]

1 ULySS is available at: http://ulyss.univ-lyon1.fr/

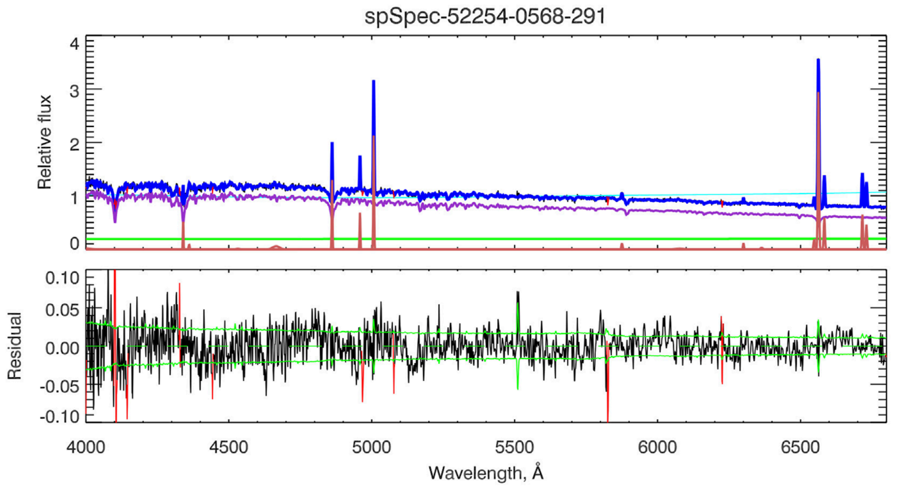

(a)

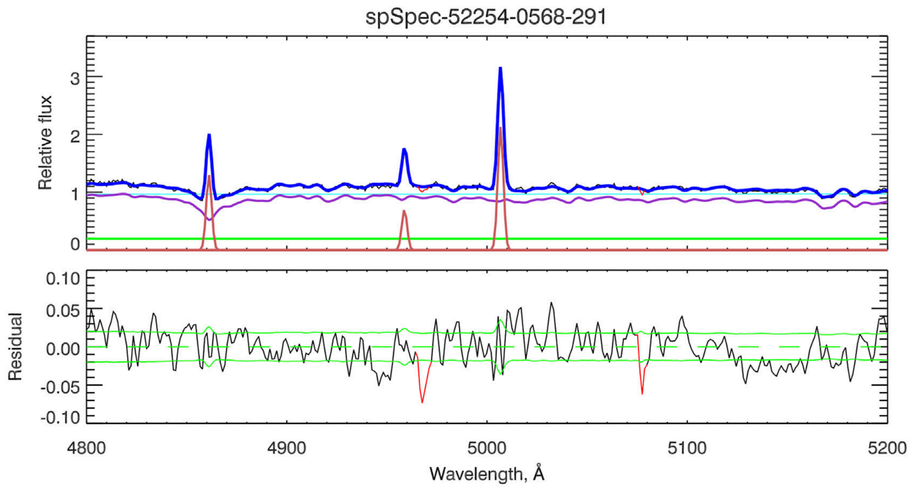

(b)

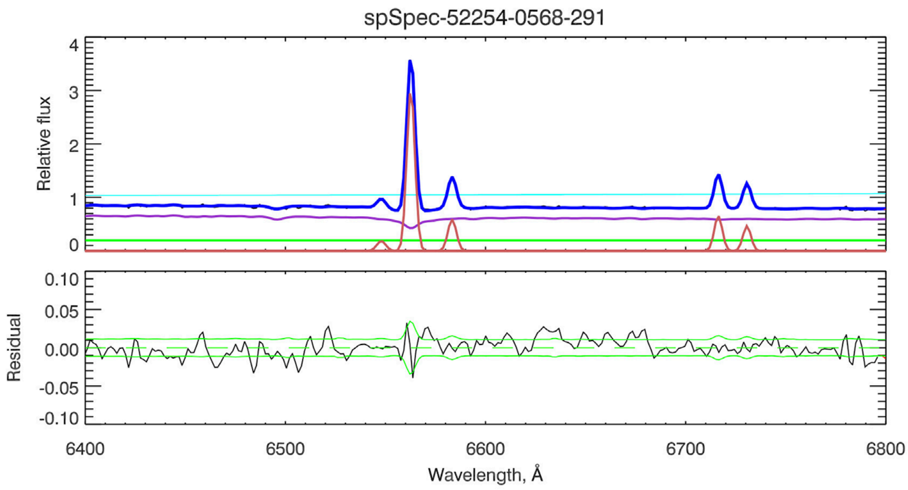

(c)

FIGURE 1
Example of the best fit in the total fitted wavelength range **(a)**, best fit of the Hβ **(b)** and Hα line **(c)** in Seyfert 2 spectra (SDSS spSpec-53089-1,381-015) using model of single Gaussian function for emission line fit. In the upper panels of the graphs, the black line represents the observed spectrum, the blue line represents the best fit model, and the red line the multiplicative polynomial, while the green, light red, and violet lines represent components of the best fit model: violet–stellar population, red–emission lines, and green–AGN continuum. The bottom panel represents residuals of the best fit (black line). The solid green lines mark the 1σ deviation, and the dashed line is the zero axis.

TABLE 1 Average flux ratios of [OIII] and [NII] with standard error of the mean (SEM), and Shapiro-Wilk test statistics (W, p), calculating with three different extinction laws. Bold p-values indicate samples consistent with a normal distribution. A probability $p \leq 0.05$ identifies distributions with significant deviations from normality.

Type	R [OIII]				R [NII]			
	No.	$R_V = 2.1$	$R_V = 3.1$	$R_V = 4.1$	No.	$R_V = 2.1$	$R_V = 3.1$	$R_V = 4.1$
Sy2	36	2.97 ± 0.02 W = 0.979 **p = 0.707**	2.98 ± 0.02 W = 0.980 **p = 0.760**	2.99 ± 0.02 W = 0.980 **p = 0.760**	37	2.98 ± 0.02 W = 0.983 **p = 0.831**	2.98 ± 0.02 W = 0.984 **p = 0.846**	2.98 ± 0.02 W = 0.984 **p = 0.846**
LINER	48	2.98 ± 0.03 W = 0.948 p = 0.035	2.98 ± 0.03 W = 0.948 p = 0.035	3.01 ± 0.04 W = 0.952 p = 0.049	47	2.96 ± 0.03 W = 0.982 **p = 0.685**	2.96 ± 0.03 W = 0.982 **p = 0.685**	2.96 ± 0.03 W = 0.983 **p = 0.701**
Composite	262	2.980 ± 0.008 W = 0.993 **p = 0.261**	2.992 ± 0.009 W = 0.993 **p = 0.258**	3.002 ± 0.009 W = 0.996 **p = 0.272**	201	2.980 ± 0.008 W = 0.993 **p = 0.452**	2.981 ± 0.008 W = 0.993 **p = 0.470**	2.981 ± 0.008 W = 0.993 **p = 0.470**
HII	1167	2.953 ± 0.005 W = 0.986 p = 2.5e-6	2.977 ± 0.006 W = 0.984 p = 3.1e-7	2.997 ± 0.006 W = 0.984 p = 3.1e-7	1486	3.044 ± 0.003 W = 0.996 p = 0.0002	3.046 ± 0.003 W = 0.996 p = 0.0002	3.051 ± 0.00 W = 0.996 p = 0.0002

ratio analysis our analyzed samples counted 37 Sy2s, 47 LINERs, 202 composites and 1,513 starbursts for flux ratio analysis.

In order to remove extreme outliers we performed sigma-clipping procedure within standard 3σ threshold. This process primarily affected the starburst sample, where approximately ~ 2.5% of objects were removed. In contrast, for other galaxy subclasses, the number of spectra remained largely unchanged after sigma clipping; either no objects were excluded, or at most one or two spectra were clipped. The final number of spectra, after sigma clipping, used for calculation of the arithmetic average and their errors are reported in the Table 1. After applying all our selection criteria and performing σ-clipping to remove outliers, we found that the *broadest emission line* in our sample exhibits a velocity dispersion of $\sigma = 149$ km s^{-1}, which corresponds to a full width at half maximum (FWHM) of 352 km s^{-1}, assuming a Gaussian profile. This value sets the upper limit for the line widths considered in our analysis and ensures consistency across all fitted components.

3.2 Extinction correction procedure

The observed emission line fluxes were corrected for interstellar reddening using the Balmer decrement, specifically the Hα/Hβ ratio.

To accurately measure the intrinsic fluxes of emission lines in our sample of galaxies, we corrected for interstellar reddening by applying an extinction correction based on the observed Balmer decrement, specifically the $H\alpha/H\beta$ ratio. This approach allows us to estimate the degree of dust extinction, which primarily affects shorter wavelengths and thereby alters the observed flux ratios of emission lines. The reddening correction was applied using the Cardelli et al. (1989) extinction.

The hydrogen Balmer lines are commonly employed to estimate the level of extinction affecting the observed emission lines of a photoionized plasma. This is because the intrinsic Balmer decrement values are largely insensitive to variations in gas temperature and density (if electron density is low, ~100 cm^{-3}). This principle holds true for H II regions that are ionized by hot stars. Deviations from this intrinsic value in the observed ratio indicate the presence of dust extinction. However, for the narrow-line regions (NLRs) of Seyfert 2 galaxies, where the ionizing spectrum is significantly harder, the intrinsic Hα/Hβ Balmer decrement is generally estimated to be in the range of 3.0–3.1. This is slightly higher than the recombination Case B value (e.g., Gaskell and Ferland, 1984; Veilleux and Osterbrock, 1987). Therefore, for HII regions we adopt intrinsic Balmer decrement value of 2.86 as expected for standard Case B recombination at $T \approx 10{,}000$ K and $n_e \approx 100$ cm^{-3}, while for other cases LINER, Composites and Seyfert galaxies, where collisional excitation, harder radiation, or dust effects may occur, the intrinsic value is assumed to be 3.1.

To quantify the extinction, we applied the reddening law, which expresses the total extinction $k(\lambda)$ as a function of wavelength:

$$k(\lambda) = a(x) + \frac{b(x)}{R_V}, \tag{1}$$

where $x = \frac{1}{\lambda}$ (in units of $\mu\mathrm{m}^{-1}$) is the inverse wavelength, while R_V presents the ratio of total-to-selective extinction, and determines the shape of the reddening law, which varies with the physical and chemical properties of the dust along the line of sight. We varied the $R_V = (2.1, 3.1, 4.1)$, to examine how different reddening assumptions affect the results for each sample (see, Table 1).

The ratio $R_V = 3.1$ is the standard value for interstellar dust in the diffuse Milky Way ISM. This value is commonly used for star-forming regions as extinction law for diffuse clouds Cardelli et al. (1989). For Seyfert 2, composite, and LINERs R_V may differ, reflecting an extinction law of different steepness. These other values are motivated by observations of AGN and similar environments, where the extinction curve often deviates from the standard Milky Way curve due to differences in the dust composition and density (Maiolino et al., 2001) stop.

The selection of different $R_V = (2.1, 3.1, 4.1)$ for AGN-related objects is supported by studies suggesting that the grain size distribution in AGN and LINER environments may differ from that in the Milky Way. Specifically, these regions may contain a larger fraction of small grains, or an increased presence of large grains, leading to variations in R_V. Observational studies of reddening curves in AGN environments often indicate steeper extinction laws, providing justification for considering values of $R_V > 3.1$.

The functions $a(x)$ and $b(x)$ were computed using the series expansions for the optical wavelength range (see Cardelli et al., 1989)

The reddening correction was applied to the observed fluxes $F(\lambda)$ of lines by using the relation:

$$R_{\mathrm{corr}} = R_{\mathrm{obs}} \times 10^{-E(B-V)k(\lambda)}, \tag{2}$$

where R is the ratio of emission lines and $E(B-V)$ is the color excess determined from the Balmer decrement (see,for e.g., Shivaei et al., 2020):

$$E(B-V) = 2.5 \times \log\left[\frac{(H\alpha/H\beta)_{\mathrm{obs}}}{(H\alpha/H\beta)_{\mathrm{int}}}\right] \times \frac{1}{k(H\beta)-k(H\alpha)} \quad \mathrm{mag.} \tag{3}$$

where: $(H\alpha/H\beta)_{\mathrm{obs}}$ is the observed flux ratio of Hα to Hβ, $(H\alpha/H\beta)_{\mathrm{int}}$ is the intrinsic flux ratio of Hα to Hβ, k(Hα) and k(Hβ) are the extinction coefficients for Hα and Hβ, respectively and $E(B-V)$ is the color excess due to reddening.

4 Results

4.1 [O III]$\lambda\lambda$4959, 5007 line ratio

The forbidden [O III] lines at 4,958.911 Å and 5,006.843 Å are emitted from transitions within the O^{2+} ion, corresponding to the transitions $2s^22p^2\ {}^1D_2 \rightarrow 2s^22p^2\ {}^3P_1$ and $2s^22p^2\ {}^1D_2 \rightarrow 2s^22p^2\ {}^3P_2$ respectively, and their ratio under the assumption of a low-density environment is theoretically expected to be 2.89 (Galavis et al., 1997), or 2.98 by including relativistic corrections to the magnetic dipole operator (Storey and Zeippen, 2000).

Observationally, some deviations have been noted: Iye et al. (1987) obtained 3.17 ± 0.04, and Leisy and Dennefeld (1996) reported 3.00 ± 0.08 (Popović et al. (2005)), 2.92 ± 0.08, Dimitrijević et al. (2007) 2.993 ± 0.014 and Laker et al. (2022) between 3.017 and 3.022.

We present our results of [OIII]$\lambda\lambda$4,959, 5,007 flux ratios for every analyzed sub-sample of NELG in the top panel of Figures 2,3, and Table 1. Table 1 reports the sample size, the [OIII]λ5,007/[OIII]λ4,959 and [NII]λ6,583/[NII]λ6,548 intensity ratio averages and their associated errors, for three extinction curves with values or $R_V = 2.1, 3.1, 4.1$. The sample averages were computed applying a sigma-clipping algorithm iteratively, continuing the process until the values converged. The errors are the error on the average (i.e., the sample standard deviation divided by the number of degrees of freedom, sample size $N-1$).

Figure 2 presents the comparison between our measurements of the average values calculated for three extinction laws ($R_V = 2.1, 3.1, 4.1$) and the theoretical values of Storey and Zeippen (2000) and Galavis et al. (1997). The statistical significance of the results was estimated by computing a z estimator defined as $z = | < ([\mathrm{OIII}]\lambda5007/[\mathrm{OIII}]\lambda5007)_{\mathrm{obs}} > - ([\mathrm{OIII}]\lambda5007/[\mathrm{OIII}]\lambda5007)_{\mathrm{theor}}|/\sigma_{\mathrm{mean}}$ which follow a Student's t distribution. We find that [OIII] line ratios correspond to theoretical prediction of Storey and Zeippen (2000) for samples Sy, LINER and composite for any of the considered values of R_V, while for HII regions this solution correspond to the cases $3.1 \leq R_V \leq 4.1$. The case $R_V = 4.1$ is marginally different from 2.98 (probability $P \sim 1-6.10^{-3}$), but definitely not consistent with 2.89.

In the Figure 3 we present the line ratio distributions for each sample (Seyfert 2, LINER, composite, and H II regions), assuming $R_V = 3.1$ for reddening corrections. The left panel displays the results for [O III], while the right panel shows the results for [N II].

We applied the Shapiro-Wilk test to assess Gaussianity of the distributions presented in the Figure 3. The test confirmed Gaussianity only for the distribution of line ratios in the composite sample, across all tested combinations: both line ratio distributions and all R_V values. For all other samples, the distributions deviate from a Gaussian profile. In our plots, the Gaussian overlay is included primarily for illustrative purposes, serving as a reference rather than an indication of an exact fit to the data.

The Figure 3 present the distribution of [OIII]$\lambda\lambda$4959, 5007 flux ratios in a form of histograms.

4.2 [N II]$\lambda\lambda$6548,6583 line ratio

The [N II] emission lines at 6,548 Å and 6,583 Å arise from transitions within the N^+ ion. Two transitions are commonly observed in astrophysical spectra: (1) $2s^22p^2\ {}^1D_2 \rightarrow 2s^22p^2\ {}^3P_1$ ([N II] λ6548.05 Å) and (2) $2s^22p^2\ {}^1D_2 \rightarrow 2s^22p^2\ {}^3P_2$ ([N II] λ6583.45 Å). These radiative transitions are forbidden in electric dipole radiation due to parity violations and inter-combination restrictions ($\Delta S = 0$). However, the [N II] λ6548 and λ6583 lines are often strong in optical spectra from low-density, photoionized regions due to the vast emitting volumes.

The critical density for collisional de-excitation of the ${}^1D_2$ level is 6.6×10^4 cm^{-3} (Osterbrock and Ferland, 2006). In environments with higher electron densities, this metastable level is more likely depopulated by electron impacts rather than by radiative transitions, causing [N II] $\lambda\lambda$ 6,548, 6,583 Å lines to be absent in spectra. These lines are often observed adjacent to the Hα line, making them useful for diagnostics in star-forming regions as well as in AGN environments.

The theoretical intensity ratio of [N II] λ6583 to [N II] λ6548 is 2.94 (e.g., Condon, 1934; Galavis et al., 1997) or 3.05 with including relativistic corrections to the magnetic dipole operator (Storey and Zeippen, 2000).

Figure 3 shows the distribution of [NII]$\lambda\lambda$6548, 6583 flux ratios for four subclasses of NELG spectra. Results of sigma-clipped average value of the distributions for each type of galaxy are presented in Table 1.

The result for starburst spectra are in a good agreement with theoretical expectation of Storey and Zeippen (2000), especially for the case of $R_V = 4.1$. Results for LINERs, composites and Sy2 are significantly lower and hence closer to theoretical values of Galavis et al. (1997), for all versions of analyzed extinction laws. The z estimators confirms a significant difference with Storey and Zeippen (2000) at a confidence level $\gtrsim 3\sigma$ in all extinction cases and for all classes save the HII nuclei. However, due to the large dispersion, Sy2 and LINER classes are only marginally in disagreement with [Storey and Zeippen (2000)]. The composite

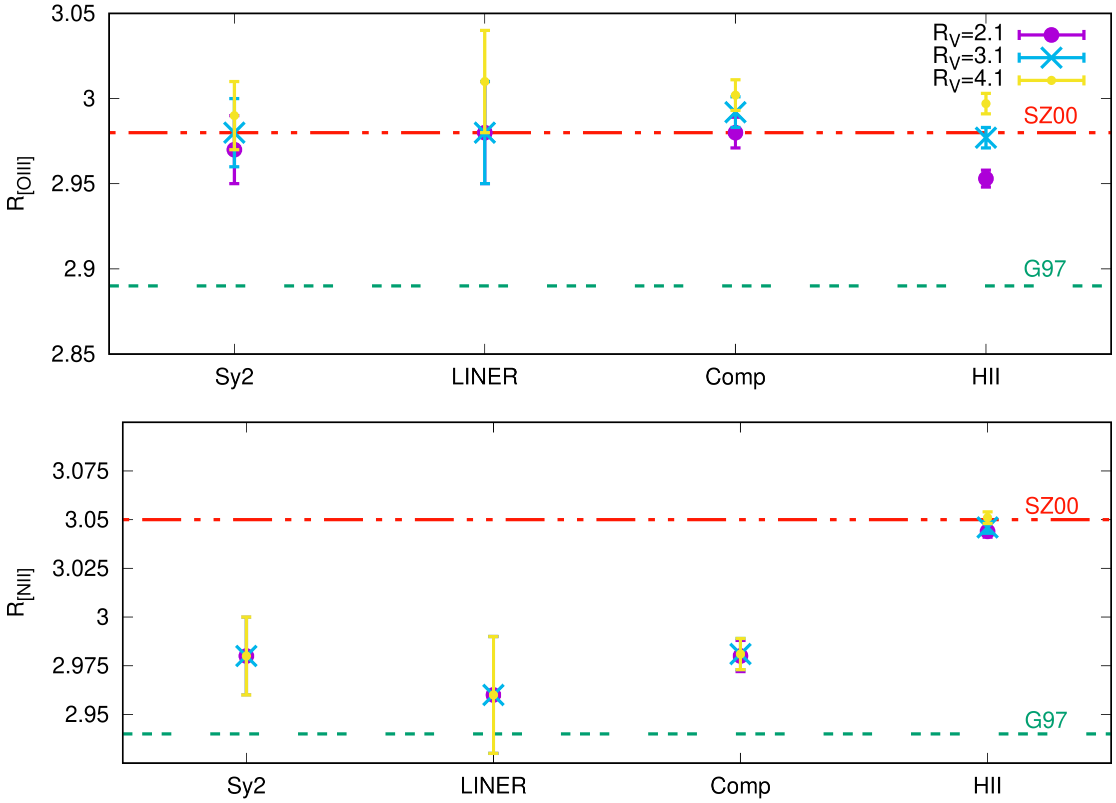

FIGURE 2
The comparison of $R_{[OIII]}$ (upper panel) and $R_{[NII]}$ (bottom panel) with the theoretical values from Storey and Zeippen (2000) and Galavis et al. (1997).

class, due to the large sample size, is in significant disagreement with both 2.94 and 3.05 (see Figure 2).

The reason could be physical and environmental conditions that can result with slight changes in [NII] line ratio as mentioned above, for example, if the density fluctuations reach values close to critical density, due to shocks (see, Rich et al., 2011). The [NII] lines are more sensitive to physical conditions then [OIII]. The highest discrepancy (3.6%) between our result and theoretical values is in the case of LINERs, where shocks are typically expected. We can conclude that our measurements are in overall agreement with theoretical predictions.

In addition to the [OIII] line ratio analysis, we also investigated the [NII] $\lambda6584/\lambda6548$ ratios across different galaxy classes and extinction laws. Unlike the case of [OIII], where all subsamples agree closely with the theoretical value of 2.98 (given by Storey and Zeippen, 2000), the results on the [NII] ratios are less straightforward to assess. Our measured [NII] ratios vary depending on both galaxy type and the adopted extinction law, spanning the interval between two commonly cited theoretical predictions in the literature: 2.94 (Galavis et al., 1997) and 3.05 (Storey and Zeippen, 2000).

To quantify the agreement between our data and theoretical expectations, we performed a two-tailed z-test for each galaxy class and extinction curve ($R_V = 2.1,\ 3.1,\ 4.1$), using both theoretical values as references. The results reveal that the H II galaxies are in best agreement with the Storey and Zeippen (2000) prediction, particularly under $R_V = 4.1$ where $p = 0.74$. In contrast, the LINERs, Seyfert 2s, and Composite galaxies show statistically significant disagreement with the Storey and Zeippen (2000), while being more consistent with the Galavis et al. (1997) value.

These deviations are plausible. The [NII] lines are more sensitive to gas density and ionization structure than [OIII], and are particularly sensitive to shock excitation and other processes in AGN-driven environments. The largest deviation is found in LINERs, where shocks are expected to play a significant role (Rich et al., 2011). Overall, the measured [NII] ratios are consistent with theoretical predictions when the environmental and excitation conditions specific to each galaxy type are considered.

5 Discussion

The observed ratios of forbidden doublet lines, such as ([N II] $\lambda6584/\lambda6548$ and ([O III] $\lambda5007/\lambda4959$, are expected to follow theoretical values in the low-density limit (≈2.96 for [N II] and ≈3.0 for [O III]) (Osterbrock, 1989). However, deviations from these values can occur due to various physical mechanisms. While reddening effects can alter the observed ratios, several intrinsic effects also play a role.

Forbidden lines arise from metastable levels and are sensitive to electron density (n_e). If the density exceeds the critical density (n_{crit}) for a given transition, collisional de-excitation suppresses the emission of the stronger line in the doublet, lowering the observed ratio

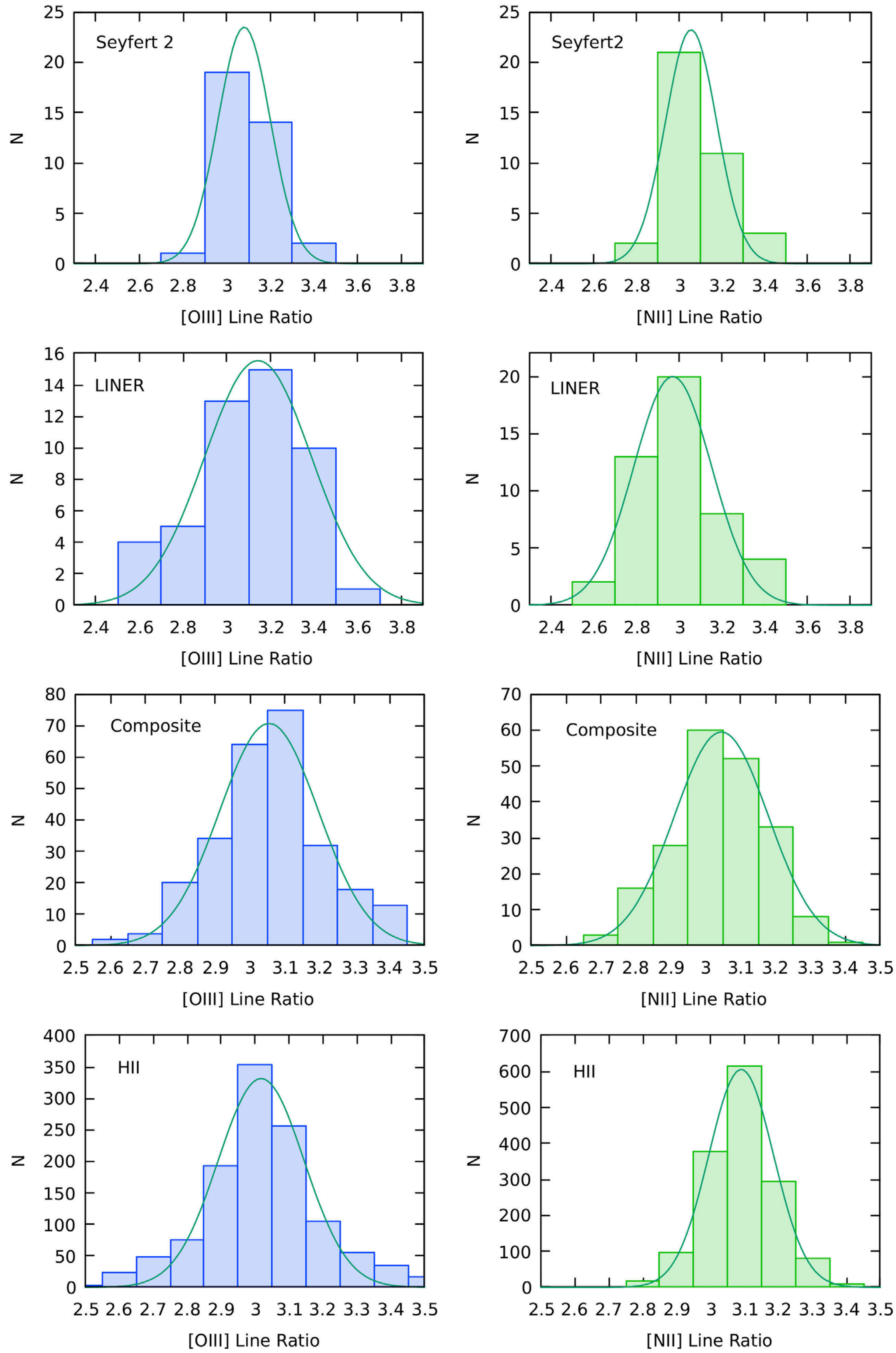

FIGURE 3
[OIII]4959,5007Å (left hand side) and [NII]$\lambda\lambda$6548,6583 (right hand side) flux ratio distribution for Sy2, LINER, composite and star-forming sample of galaxies, respectively. All histograms have over-plotted the Gaussian fit, showing the position of the mean value of normal distributions.

(Osterbrock and Ferland, 2006). For $[NII]$ $\lambda6584, 6548$ critical density is 6.6×10^4, while for $[OIII]$ $\lambda5007, 4959$ is 6.8×10^5. For low-density regions ($n_e \ll n_{\mathrm{crit}}$), line ratios follow theoretical values. However, in AGN narrow-line regions (NLRs) or supernova remnants, shocks may increase density and suppress the strongest line via collisional de-excitation (Rich et al., 2011; Veilleux and Osterbrock, 1987).

Forbidden transitions are typically optically thin, but in dense regions self-absorption can suppress the strongest line, while resonant scattering increases photon escape times (Gaskell, 2017). These effects can modify the doublet ratio, particularly in high-density ionized clouds.

The interpretation of emission line ratios in galaxies requires careful consideration of both intrinsic ionization conditions and the effects of reddening. The total-to-selective extinction parameter, R_V, influences the reddening correction applied to observed emission lines and, consequently, the derived line ratios.

The results in Table 1 indicate that for most galaxy types, the [O III] and [N II] line ratios exhibit only minor variations with changes in R_V, typically within the range of 0.01–0.02. However, LINERs show a slightly larger variation for the case of [O III] line ratio. This suggests that LINERs may have different dust properties or ionization conditions compared to other galaxy subclasses.

The primary factors contributing to these trends include the fact that LINERs are commonly found in evolved, passive galaxies, where dust grain size distributions and compositions may differ from those in star-forming regions. Unlike H II regions or Seyfert galaxies, LINERs often exhibit lower ionization parameters, which could make their line ratios more sensitive to subtle extinction effects. Some LINERs show evidence of shock-driven ionization Rich et al. (2011), which can alter the relative strengths of forbidden lines and make them more sensitive to dust corrections.

Seyferts and LINERS may also need additional semi broad component in the model. Preliminary tests from re-fitting Seyfert 2 sample with a two-component model (narrow + semi-broad) reveal that the inclusion of an additional semi-broad Gaussian often results in an increase in the measured line ratios. A close inspection of the line profiles shows that in many cases, the additional semi broad component either (1) significantly overlaps with neighboring lines such as Hα and [NII] due to its broad width (clearly exceeding the wavelength spacing between lines) or (2) contributes so little flux that it is practically negligible.

Given this situation, we conclude that adopting a two-component model for the [NII]+Halpha would either (a) lead to a substantial loss of usable spectra due to the overlap criterion being violated, or (b) require ignoring the overlap in faint-component cases, which undermines methodological consistency. Conversely, in cases where the semi-broad component is very faint, its impact is minimal, and the spectrum could arguably remain. However, this raises a concern about "uniform treatment": either we apply a strict overlap rejection to all cases regardless of flux contribution, which would severely reduce the sample size (already limited), or we introduce subjective thresholds, risking inconsistent selection. If we retain the two-component model, then the overlap criterion is violated in many cases where the semi broad component is significant. Thus, for the purpose of maintaining a statistically significant and uniformly treated sample, we favor the use of a single-component model uniformly for all spectra, regardless of whether a second component could be locally justified.

In contrast to LINERs, Seyfert 2 (Sy2) galaxies and composite galaxies exhibit greater stability in their line ratios across different values of R_V. The doublet ratios in Seyferts remain nearly unchanged, suggesting that their reddening properties are well described by a standard Milky Way-like extinction curve with $R_V \approx 3.1$. Similarly, composite galaxies and H II regions show minimal deviation, indicating that their reddening corrections do not significantly alter their observed emission line ratios.

H II regions, however, exhibit a slight increase in the [O III] and [N II] doublet ratios at $R_V = 4.1$, suggesting that in highly star-forming regions, the dust properties may differ from those in AGN-dominated environments. This is consistent with previous studies showing that star-forming galaxies often exhibit slightly higher R_V values due to their dense, multi-phase ISM (see, Calzetti et al., 2000 where they find $R_V = 4.05 \pm 0.8$ for HII regons).

The observed trends in forbidden line ratios provide insights into the evolutionary stages and ionization mechanisms of different galaxy types. The distinct behavior of LINERs suggests that they may represent a transition phase in galaxy evolution, where ionization is no longer dominated by young stars but rather by hot post-AGB stars, weak AGN, or shock processes.

Our results demonstrate that the impact of reddening corrections on emission line ratios is generally small but not negligible, particularly in LINERs. They exhibit a stronger dependence on R_V, suggesting possible differences in dust properties or ionization mechanisms. The relative stability of Seyferts, composites, and H II regions under varying R_V reinforces the robustness of extinction corrections in these systems.

These findings emphasize the importance of considering both extinction corrections and underlying astrophysical processes when interpreting emission line ratios in different galaxy types.

6 Conclusion

Theoretical values obtained for transition probabilities of emission lines could be in some cases tested only in astrophysical conditions. In the spectra of narrow emission line galaxies forbidden emission lines such as [OIII]$\lambda\lambda$4959,5007 and [NII]$\lambda\lambda$6548, 6583 line doublets are very strong, and present good candidates for testing theoretical expectations.

In this study, we investigated the ratios of the optical forbidden emission lines [OIII]$\lambda\lambda$4959,5007 and [NII]$\lambda\lambda$6548, 6583 in a volume limited sample of ~ 1500 spectra from Seyfert 2, LINER, composite and star-forming galaxies ($0.01 \leqslant z \leqslant 0.05$).

The latest theoretical prediction for [OIII]$\lambda\lambda$4959,5007 line ratio is ~ 2.98, while for the case of [NII]$\lambda\lambda$6548,6583 line ratio it is ~ 3.05 (Storey and Zeippen, 2000).

In summary, our results demonstrate following: (i) The impact of reddening corrections on emission line ratios is generally small but not negligible, particularly in LINERs; (ii) LINERs exhibit a stronger dependence on R_V, suggesting possible differences in dust properties or ionization mechanisms; (iii) the relative stability of Seyferts, composites, and H II regions while varying R_V reinforces the robustness of extinction corrections in these cases.

We find that [OIII] line ratios correspond to theoretical prediction of Storey and Zeippen (2000) for samples Sy, LINER and composite in case of $2.1 \leq R_V \leq 3.1$, while for HII regions this solution correspond to $3.1 \leq R_V \leq 4.1$. For [N II] lines, the theoretical predictions of Storey and Zeippen (2000) align with H II regions within the same R_V range as [OIII]. However, for Seyfert, LINER, and composite galaxies, while the [NII] ratio does not exhibit significant variation with R_V, its measured values are slightly lower than those predicted by Storey and Zeippen (2000) and instead closer to the predictions of Galavis et al. (1997). This discrepancy may suggest that the physical and environmental conditions of the regions where [NII] originates differ between these three galaxy types and HII regions, potentially reflecting variations in electron density, ionization mechanisms, or gas composition.

Our analysis is in a good agreement with theoretical expectations and results from previous works. The measured [O III] and [N II] flux ratios across different galaxy subclasses remain largely consistent with theoretical predictions, particularly for Seyfert 2, composite galaxies, and H II regions. However, the most notable discrepancy was observed in [N II] ratio for the case of LINERs, but still remains within theoretical calculations.

Additionally, we find that the small differences observed among the four subclasses could be linked to variations in the physical conditions of their inner regions. Such differences include electron density, ionization parameter, and dust properties, all of which can influence the reddening corrections applied to emission line ratios. These effects, in turn, can lead to subtle modifications in the observed line profiles, particularly in LINERs, where the ionization mechanisms are less uniform compared to Seyfert galaxies or H II regions.

Our results reinforce the importance of considering both reddening effects and intrinsic galaxy properties when interpreting emission-line diagnostics, particularly in low-ionization systems like LINERs, where multiple ionization sources contribute to the observed spectra.

Data availability statement

The raw data supporting the conclusions of this article will be made available by the authors, without undue reservation.

Author contributions

NB: Conceptualization, Data curation, Formal Analysis, Funding acquisition, Investigation, Methodology, Project administration, Resources, Software, Supervision, Validation, Visualization, Writing – original draft. EB: Conceptualization, Formal Analysis, Investigation, Methodology, Writing – original draft. PM: Supervision, Validation, Visualization, Writing – original draft. LP: Supervision, Validation, Writing – original draft.

Funding

The author(s) declare that financial support was received for the research and/or publication of this article. This work is supported by the Ministry of Science, Technological Development and Innovation of the Republic of Serbia, contract No. 451–03–136/2025-03/200002.

Funding for the Sloan Digital Sky Survey (SDSS) and SDSS-II has been provided by the Alfred P. Sloan Foundation, the Participating Institutions, the National Science Foundation, the U.S. Department of Energy, the National Aeronautics and Space Administration, the Japanese Monbukagakusho, and the Max Planck Society, and the Higher Education Funding Council for England. The SDSS Web site is http://www.sdss.org/. The SDSS is managed by the Astrophysical Research Consortium (ARC) for the Participating Institutions. The Participating Institutions are the American Museum of Natural History, Astrophysical Institute Potsdam, University of Basel, University of Cambridge, Case Western Reserve University, The University of Chicago, Drexel University, Fermilab, the Institute for Advanced Study, the Japan Participation Group, The Johns Hopkins University, the Joint Institute for Nuclear Astrophysics, the Kavli Institute for Particle Astrophysics and Cosmology, the Korean Scientist Group, the Chinese Academy of Sciences (LAMOST), Los Alamos National Laboratory, the Max-Planck-Institute for Astronomy (MPIA), the Max-Planck-Institute for Astrophysics (MPA), New Mexico State University, Ohio State University, University of Pittsburgh, University of Portsmouth, Princeton University, the United States Naval Observatory, and the University of Washington.

Acknowledgments

We acknowledge the help of Philippe Prugniel in the sample selection process. We also acknowledge Samir Salim and Martin Gaskell for their help and useful comments.

Conflict of interest

The authors declare that the research was conducted in the absence of commercial or financial relationships that could be construed as a potential conflict of interest.

The reviewer DB declared a shared affiliation with the author PM to the handling editor at the time of review.

The author(s) declared that they were an editorial board member of Frontiers, at the time of submission. This had no impact on the peer review process and the final decision.

Generative AI statement

The author(s) declare that no Generative AI was used in the creation of this manuscript.

Publisher's note

References

Abazajian, K. N., Adelman-McCarthy, J. K., Agüeros, M. A., et al. (2009). *ApJS* 182, 543. doi:10.1088/0067-0049/182/2/543

Baldwin, J. A., Phillips, M. M., and Terlevich, R. (1981). *Publ. Astronomical Soc. Pac.* 93, 5. doi:10.1086/130766

Binette, L., Magris, C. G., Stasińska, G., and Bruzual, G. (1994). 292. *A&A,* 13.

Bon, E., Zucker, S., Netzer, H., Marziani, P., Bon, N., Jovanović, P., et al. (2016). *ApJS* 225, 29. doi:10.3847/0067-0049/225/2/29

Bon, N., Popović, L. Č., and Bon, E. (2014). Efficiency tests for estimating the gas and stellar population parameters in Type 2 objects. *Adv. Space Res.* 54, 1389–1400. doi:10.1016/j.asr.2014.06.040

Byler, N., Dalcanton, J. J., Conroy, C., Johnson, B. D., Choi, J., Dotter, A., et al. (2019). Self-consistent Predictions for LIER-like Emission Lines from Post-AGB Stars. *AJ* 158, 2. doi:10.3847/1538-3881/ab1b70

Calzetti, D., Armus, L., Bohlin, R. C., Kinney, A. L., Koornneef, J., and Storchi-Bergmann, T. (2000). The dust content and opacity of actively star-forming galaxies. *Astrophysical J.* 533, 682–695. doi:10.1086/308692

Cardelli, J. A., Clayton, G. C., and Mathis, J. S. (1989). The relationship between infrared, optical, and ultraviolet extinction. *APJ* 345, 245. doi:10.1086/167900

Condon, E. U. (1934). The absolute intensity of the nebular lines. *APJ* 79, 217. doi:10.1086/143530

Dimitrijević, M. S., Popović, L. Č., Kovačević, J., Dačić, M., and Ilić, D. (2007). *MNRAS* 374, 1181. doi:10.1111/j.1365-2966.2006.11238.x

Dojčinović, I., Kovačević-Dojčinović, J., and Popović, L. Č. (2023). *Adv. Space Res.* 71, 1219. doi:10.1016/j.asr.2022.04.041

Galavis, M. E., Mendoza, C., and Zeippen, C. J. (1997). Atomic data from the IRON Project: XXII. Radiative rates forforbidden transitions within the ground configuration of ions inthe carbon and oxygen isoelectronic sequences. *A and AS* 123, 159–171. doi:10.1051/aas:1997344

Gaskell, C. M. (2017). *MNRAS* 467, 226. doi:10.1093/mnras/stx094

Gaskell, C. M., and Ferland, G. J. (1984). Theoretical hydrogen-line ratios for the narrow-line regions of active galactic nuclei. *PASP* 96, 393. doi:10.1086/131352

Iye, M., Ulrich, M.-H., and Peimbert, M. (1987). High resolution spectrum of the starburst galaxy Tololo 1924-416 (=ESO 338-IG04). *Astronomy and Astrophysics* 186, 84–94.

Kauffmann, G., Heckman, T. M., Tremonti, C., Brinchmann, J., Charlot, S., White, S. D. M., et al. (2003). The host galaxies of active galactic nuclei. *MNRAS* 346, 1055–1077. doi:10.1111/j.1365-2966.2003.07154.x

Kewley, L. J., Dopita, M. A., Sutherland, R. S., Heisler, C. A., and Trevena, J. (2001). Theoretical modeling of starburst galaxies. *APJ* 556, 121–140. doi:10.1086/321545

Kewley, L. J., Groves, B., Kauffmann, G., and Heckman, T. (2006). The host galaxies and classification of active galactic nuclei. *MNRAS* 372, 961–976. doi:10.1111/j.1365-2966.2006.10859.x

Koleva, M., Prugniel, P., Bouchard, A., and Wu, Y. (2009). ULySS: a full spectrum fitting package. *A and A* 501, 1269–1279. doi:10.1051/0004-6361/200811467

Laker, M. A., Camacho, C. D., Jones, D., and Moody, J. (2022). The flux ratio of the [OIII]λλ5007,4959 doublet with redshift. *Symmetry* 14, 266. doi:10.3390/sym14020266

Leisy, P., and Dennefeld, M. (1996). *A and As*, 116, 95.

Maiolino, R., Marconi, A., and Oliva, E. (2001). *Astron Astrophys.* 365, 37–48. doi:10.1051/0004-6361:20000012

Osterbrock, D. E. (1989). Astrophysics of gaseous nebulae and active galactic nuclei, 101, 341. Available online at: https://ui.adsabs.harvard.edu/abs/1989agna.book

Osterbrock, D. E., and Ferland, G. J. (2006). *Astrophysics of gaseous nebulae and active galactic nuclei*. 2nd edn. Sausalito, California: University Science Books.

Popović, L. Č., Dimitrijević, M. S., Bon, E., and Dačić, M. (2005). Publications of the astronomical society. *Rudjer Boskovic* 5, 247.

Rich, J. A., Kewley, L. J., and Dopita, M. A. (2011). *APJ* 734, 87. doi:10.1088/0004-637X/734/2/87

Sánchez-Blázquez, P., Peletier, R. F., Jiménez-Vicente, J., et al. (2006). *MNRAS* 371, 703. doi:10.1111/j.1365-2966.2006.10699.x

Shivaei, I., Reddy, N., Rieke, G., Shapley, A., Kriek, M., Battisti, A., et al. (2020). The MOSDEF survey: the variation of the dust attenuation curve with metallicity. *APJ* 899, 117. doi:10.3847/1538-4357/aba35e

Stasińska, G., Vale Asari, N., Cid Fernandes, R., Gomes, J. M., Schlickmann, M., Mateus, A., et al. (2008). Can retired galaxies mimic active galaxies? clues from the sloan digital sky survey. *MNRAS* 391, L29– L33. doi:10.1111/j.1745-3933.2008.00550.x

Storey, P. J., and Zeippen, C. J. (2000). Theoretical values for the [O iii] 5007/4959 line-intensity ratio and homologous cases. *MNRAS* 312, 813–816. doi:10.1046/j.1365-8711.2000.03184.x

Strauss, M. A., Weinberg, D. H., Lupton, R. H., Narayanan, V. K., Annis, J., Bernardi, M., et al. (2002). Spectroscopic target selection in the sloan digital Sky survey: the main galaxy sample. *AJ* 124, 1810–1824. doi:10.1086/342343

Vazdekis, A., Sánchez-Blázquez, P., Falcón-Barroso, J., Cenarro, A. J., Beasley, M. A., Cardiel, N., et al. (2010). Evolutionary stellar population synthesis with MILES - I. The base models and a new line index system. *MNRAS* 404, 1639–1671. doi:10.1111/j.1365-2966.2010.16407.x

Veilleux, S., and Osterbrock, D. E. (1987). Spectral classification of emission-line galaxies. *Astrophysical J. Suppl. Ser.* 63, 295. doi:10.1086/191166